Dovepress

ORIGINAL RESEARCH

Integrated Metabolomics and Network Pharmacology Study on the Mechanism of *Rehmanniae radix* Extract for Treating Thrombosis

Hongling Du[1–3], Shunjie Zhang[1], Kezhu Yuan[4], Zhirui Yang[5], Mingquan Wu [4]

[1]Department of Pharmacy, West China Hospital, Sichuan University, Chengdu, Sichuan, People's Republic of China; [2]Department of Pharmacy, Sichuan Public Health Clinical Center, Chengdu, Sichuan, People's Republic of China; [3]State Key Laboratory of Southwestern Chinese Medicine Resources, Pharmacy School, Chengdu University of Traditional Chinese Medicine, Chengdu, Sichuan, People's Republic of China; [4]Department of Pharmacy, Sichuan Orthopedic Hospital, Chengdu, Sichuan, People's Republic of China; [5]Department of Nuclear Medicine, Chengdu Second People's Hospital, Chengdu, Sichuan, People's Republic of China

Correspondence: Mingquan Wu, Department of Pharmacy, Sichuan Orthopedic Hospital, Chengdu, Sichuan, People's Republic of China, Email 18782976939@163.com

Background: *Rehmanniae Radix* (RR) has received attention for its antithrombotic effect. However, few studies have independently explored the bioactive components responsible for its antithrombotic bioactivity and the potential mechanism. We aimed to reveal the antithrombotic mechanisms of RR by using metabolomics integrated with network pharmacology.
Methods: A thrombosis model was established by intraperitoneal injection of type I carrageenan in rats, and antithrombotic function was evaluated at different doses of RR. Metabolomics was used to identify the differential metabolites in the serum. Network pharmacology was then applied to identify the potential targets for the antithrombotic activity of the RR. An integrated network of metabolomics and network pharmacology was constructed using Cytoscape. Finally, key targets were verified using molecular docking.
Results: RR at 5.4 g/kg significantly alleviated the thrombosis. Thirteen potentially significant metabolites were involved in the therapeutic effects of RR against thrombosis, most of which were regulated for recovery after RR treatment. An integrated analysis of metabolomics and network pharmacology showed that the antithrombosis effect of RR was closely associated with the regulation of PLA2G2A, PTGS1, ALOX5, and CYP2C9. Molecular docking showed high affinity between the key targets and components of RR. We speculated that the components of RR, such as catalpol, ferulic acid methyl ester, and methyl 4-hydroxycinnamate, might act on key proteins, including PLA2G2A, PTGS1, and ALOX5, to exert antithrombosis effects.
Conclusion: This study confirmed the antithrombotic effect of high-dose RR, revealed the antithrombotic mechanism and potential material basis, and laid the foundation for the antithrombotic clinical application of RR. Furthermore, it provides a successful case reference for screening natural herbal components and exploring their potential pharmacological mechanisms.
Keywords: *Rehmanniae radix*, antithrombotic effects, metabolomics, network pharmacology

Introduction

Thrombosis is caused by vascular endothelial cell injury, abnormal blood flow, and increased blood coagulation, etc. Thrombosis is a key link of cardiovascular diseases and a main cause of death and disability worldwide, making it a major healthcare challenge.[1] According to the reports from World Health Organization, about 16 million people die from thrombotic diseases each year worldwide, and the deaths in China account for 51% of the total deaths. Thrombosis formation is modulated by factors, including the thrombogenicity of plaques and blood, local hemorheology and proinflammatory factors.[2] Once thrombosis has formed, long-term control is required, which greatly reduces the quality of life of the patients. The first-line drugs for thrombosis treatment, including heparin, urokinase, aspirin, and clopido-grel, have limited efficacy, obvious side effects, and high toxicity. For example, heparin is primarily used to treat recent thrombotic diseases, but it can lead to complications such as bleeding and thrombocytopenia. Urokinase, while effective at activating fibrinolytic enzymes, also degrades fibrinogen in the bloodstream. This medication must be administered

intravenously, which can limit patient adaptability. Additionally, aspirin and clopidogrel are associated with the risk of gastrointestinal bleeding.[3] Therefore, there is an urgent need to focus on traditional Chinese medicine (TCM) and find safe and effective Chinese herbal medicine for the clinical treatment of thrombosis.

Rehmanniae Radix (RR), the dried tuberous root of *Rehmannia glutinosa* Libosch., has been a common herb used in China for over 2000 years. RR is known to play an important role in some classic formulas to treat thrombi, such as the Siwu decoction and Xuefu Zhuyu decoction.[4] Currently pharmacological evidence suggests the promising efficacy of RR against thrombosis.[5–7] The antithrombotic bioactivity of RR has been validated for thousands of years of clinical use in China.[5] In a recent study, Gong et al also validated the antithrombotic bioactivity of RR extract, but the effect was significantly decreased after processing.[6] Then the oligosaccharides and iridoid glycosides of RR extract were preliminarily traced based on multidimensional spectrum-effect relationship analysis.[7] However, the substantial basis of RR treating thrombus and the underlying mechanism remain unclear.

Metabolomics, a powerful approach used to supervise the changes of all physiopathological metabolites in the whole organism, can elucidate the metabolic mechanism of TCM, which is in line with the holistic characteristic of TCM in treating diseases.[8] Network pharmacology constructs the "compound-target-pathway" network based on public databases to qualitatively predict the material basis, associated targets, and signaling pathways of TCM.[9,10] The integration of two strategies has been applied in the field of TCM, including drug target discovery, efficacy evaluation, and mechanism investigation. Therefore, it is desirable to integrate metabolomics with network pharmacology. In the present study, untargeted metabolomics was applied to determine the modulatory effects of RR on thrombosis and to identify essential metabolites. A network pharmacology study was performed to predict the active compounds, key targets, and signaling pathways of RR in thrombosis. Furthermore, interactions between the active compounds and key targets were evaluated via molecular docking. Collectively, this strategy will hopefully contribute to a better understanding of the therapeutic effect of RR on thrombosis treatment, including the material basis, critical targets, signaling pathways, and metabolite changes.

Material and Methods

Reagents and Materials

RR (192031) was purchased from Sichuan Haorentang Co. Ltd (Chengdu, China), authenticated by Prof. He Tu from Chengdu University of Traditional Chinese Medicine, and kept in the preparation center sample showroom of Chengdu University of Traditional Chinese Medicine (CDTCM20221012-1).

Type I carrageenan (C804872) was obtained from MACKLIN (Shanghai, China). Enteric-coated aspirin tablets (20130078) were produced by Bayer (Leverkusen, Germany). Enzyme-linked immunosorbent assay (ELISA) kits, including interleukin-6 (IL-6, A301B90421) and tumor necrosis factor-alpha (TNF-α, A38290222), were obtained from MultiSciences (Hangzhou, China); endothelin-1 (ET-1, 20191223) was purchased from Mlbio (Shanghai, China); and nitric oxide (NO, KXZCL8KTW5) was purchased from Elabscience (Wuhan, China). Acetonitrile and methanol (MS grade) were purchased from Merck (Darmstadt, Germany). Formic acid (MS-grade) was purchased from Dikma (Beijing, China). Leucine enkephalin was purchased from Waters (Milford, USA).

RR Extract Preparation

First, 300 g of RR was soaked in water (14 times the volume, 4200 mL) for 30 min and then extracted twice with boiling water (each time for 2 h). After filtration through gauze, the filtrates were mixed and evaporated to dryness. All samples were stored at 4°C.

Four iridoid glycosides (catalpol, aucubin, rehmannioside D, and ajugol) of RR extracts were characterized by high-performance liquid chromatography (HPLC; e2695, Waters, Milford, USA). Separation was performed on an Osaka Soda CAPCELL C18 Column (4.6 × 250 mm, 5 μm). The mobile phases were acetonitrile (A) and 0.1% phosphoric acid (B), and the solvent gradient was as follows: 0 – 15 min, 1% A; 15–16 min, 1% – 4.5% A; and 16–35 min, 4.5% A. The column temperature was 25°C, injection volume was 10 μL, and flow rate was 1.0 mL/min.

Animal Study

All experimental procedures were approved by the Committee on the Ethics of Animal Experiments of the Chengdu University of Traditional Chinese Medicine (licensed CDU2023S124). All animal experiments were performed by strictly complying with the guidelines for the Protection and Use of Experimental Animals of the Ministry of Science and Technology of China. Male Sprague-Dawley rats (200 ± 20 g) with free access to food and water were purchased from Chengdu Dossy Experimental Animals Co., Ltd. (Chengdu, China). The room temperature was 22 ± 1°C and the relative humidity was adjusted to 45%. After one week of acclimation, the rats were randomly divided into six groups: (1) normal control group (n = 10); (2) model group (n = 10); (3) enteric-coated aspirin treatment group (AP, n = 10); and (4–6) low-, middle-, and high-RR treatment groups (RR-L, RR-M, and RR-H, n = 10, respectively). Normal saline was administered to both control and model groups. The dosage of RR extract was converted according to the adult dosage of RR pills in the Chinese Pharmacopoeia (2020 edition) and body surface area.[11] The RR-L, RR-M, and RR-H group were treated with RR extract at 1.35, 2.7, and 5.4 g/kg, respectively. The AP group was administered enteric-coated aspirin (20 mg/kg).[6,12]

After intragastric drug administration for seven days, rats in the model, AP, RR-L, RR-M, and RR-H groups were intraperitoneally injected with type I carrageenan to induce tail thrombosis. Each group of rats was intragastrically administered different drugs for another two days. All rats were euthanized with pentobarbital sodium (i.v.) for the collection of blood samples via the abdominal aorta, ear, and carotid aorta tissue after the last drug administration. Blood samples were collected in either ordinary serum tubes or sodium citrate-containing anticoagulant tubes for the collection of serum and plasma, respectively, followed by centrifugation (3600 rpm at 4°C for 10 min).[13]

Pharmacodynamic Research

After modeling, the rat ears and tails turned black at 48 h, with varying degrees of swelling and thrombosis; then, the tail thrombus lengths were measured at 24, 36, and 48 h. The collected ear tissue and carotid aortas were preserved for hematoxylin-eosin (HE) staining.[14] The collected plasma was used for coagulation test, which was determined by automatic coagulation analyzer following standard operating protocols in medical laboratory. The serum levels of TNF-α, IL-6, ET-1, and NO were determined by ELISA, with protocols strictly followed.

Serum Sample Preparation

The serum samples were thawed before data acquisition; 600 μL of pre-cooled methanol was added to 200 μL of serum sample, vortexed for 30s, and centrifuged (13,000 rpm) at 4°C for 10 min;[13] the supernatant was transferred to a 5-mm tube for analysis. A pooled sample for quality control (QC) was obtained by mixing 10 μL of each serum sample and prepared using the aforementioned method for optimization of LC-MS conditions and method validation.[8]

UPLC Q-TOF/MS Analysis

Metabolomics was performed using a Waters Acquity UPLC system (Waters, Milford, USA) coupled with a Xevo G2-XS Q-TOF (Waters, Manchester, UK). Chromatographic separations were performed on an ACQUITY UPLC HSS T3 C18 column (2.1 × 100 mm, 1.8 μm) at 40°C. The mobile phases were 0.1% formic acid in water (A) and 0.1% formic acid in acetonitrile (B). The gradient elution was set as follows: 0–9 min, 95% – 30% A; 9–16 min, 30% – 0% A; 16–20 min, 0% A; 20–20.5 min, 0% – 95% A; 20.5–23 min, 95% A. The injection volume was 3 μL and the flow rate was 0.3 mL/min.

The MS conditions were as follows: capillary voltage, +3 kV (positive ion mode) and –2.5 kV (negative ion mode); ion source temperature, 140°C; gas temperature, 450°C; cone voltage, 40 V; cone gas flow, 50 $L \cdot h^{-1}$; desolvation gas flow, 800 $L \cdot h^{-1}$; collision energy, 10–45 V; scanning interval, 0.2 s. Leucine enkephalin solution was used in the lockmass. The mass range was 50–1200 m/z, and the data acquisition mode was 3D data acquisition in the continuum mode.

Metabolomics Data Analysis

Raw data were collected using the MassLynx software (v4.1, Waters, Milford), and peak detection, alignment, and area normalization were performed by the Application Manager. After normalization, data matrix was established and saved in

CSV format based on accurate molecular weight, retention time, and normalized peak area, then imported into SIMCA P14.0 software for multivariate statistical analysis, including principal component analysis (PCA) and orthogonal partial least-squares discrimination analysis (OPLS-DA).[15] The metabolites were identified by comparing the mass-to-charge ratio (m/z), fragmentation, and other related information with data from Human Metabolome Database (HMDB, http://www.hmdb.ca/), Kyoto Encyclopedia of Genes and Genomes (KEGG, http://www.hmdb.ca/), and METLIN (http://metlin.scripps.edu/) databases, and the mass error was controlled within 10 ppm.[16] The MetaboAnalyst 5.0 (https://www.metaboanalyst.ca/) was used for metabolic pathway enrichment analysis.[17]

Network Pharmacology Study

Compounds in RR were screened in the TCMSP (http://tcmspw.com/tcmsp.php), TCMID (http://47.100.169.139/tcmid/), and BATMAN-TCM (http://bionet.ncpsb.org/batman-tcm/) databases with oral bioavailability ≥ 30%, drug-likeness ≥ 0.18, and Lipinski's Rule of Five.[18,19] Potential target genes of RR compounds were widely searched from TCMSP and BATMAN-TCM and predicted using SwissTargetPrediction database (http://www.swisstargetprediction.ch/). Candidate genes of thrombosis were screened using the GeneCards database (http://www.genecards.org). The overlapping genes were considered potential targets of RR against thrombosis and were imported into UniProt (http://www.uniprot.org/) to standardize the gene and protein names. Gene Ontology (GO) and Kyoto Encyclopedia of Genes and Genomes (KEGG) pathway enrichment of potential targets were analyzed using DAVID (https://david.ncifcrf.gov/). The compound-target-pathway network was constructed using STRING (version 11.5, https://www.string-db.org/) and Cytoscape. The identified differential metabolites in metabolomics were imported into MBrole (http://csbg.cnb.csic.es/mbrole2/) for interactive proteins and a metabolite-target network was established using Cytoscape. Key metabolites, targets, and related compounds were identified using the merge function in Cytoscape.

Molecular Docking

3D structures of catalpol (PubChem CID: 91520), ferulic acid methyl ester (PubChem CID: 5357283), methyl 4-hydroxycinnamate (PubChem CID: 5319562), and rehmaionoside C (PubChem CID: 11740990) were obtained from PubChem (https://pubchem.ncbi.nlm.nih.gov/). The crystal structures of four protein including recombinant phospholipase A2, Group IIA (PLA2G2A, PDB ID: 1APY), cytochrome P450 family 2 subfamily C member 9 (CYP2C9, PDB ID: 5×23), prostaglandin-endoperoxide synthase 1 (PTGS1, PDB ID: 6Y3C) and recombinant arachidonate-5-lipoxygenase (ALOX5, PDB ID:3V99) were acquired from the RCSB Protein Data Bank (https://www.rcsb.org/). Compounds and proteins were converted from their native format to pdbqt format, water molecules were deleted, and hydrogen atoms were added using AutoDockTools 1.5.6. Molecular docking was performed using Lamarckian genetic algorithm. The conformation with the lowest binding energy was saved. All docking parameters were the default values.

Statistics

Data were expressed as means ± standard deviation (SD). Comparisons between groups were conducted using one-way ANOVA combined with post hoc testing using SPSS 26.0. GraphPad Prism (version 8.0) was used for graphic presentation. $P < 0.05$ indicated statistical significance.

Results

Quantitative Determination of Catalpol, Rehmannioside D, Aucubin, and Ajugol in RR Extract

It is suggested that the main material basis for the antithrombotic activity of RR is iridoid glycosides, among which catalpol and rehmannioside D are critical markers for quality control.[11] Aucubin had obvious inhibitory effect on thrombus formation in zebrafish.[20] Ajugol was reported to be a main material basis of the antithrombotic activities of RR.[7] Thus, catalpol, rehmannioside D, aucubin, and ajugol were chosen as the representative compounds in content determination for clarifying the key substantial basis of RR extract. Four representative iridoid glycosides were identified by comparing their retention time and UV spectra with those of the standard compounds. Representative HPLC chromatograms were shown in Figure S1. The

calibration curve equations with regression values for the four compounds were as follows: catalpol (y = 715959x – 116484, r = 1.0000), aucubin (y = 873619x – 4240.6, r = 0.9997), rehmannioside D (y = 668021x – 16620, r = 0.9999), and ajugol (y = 360726x – 13204, r = 0.9998). The contents of catalpol, aucubin, rehmannioside D, and ajugol were 44.85 ± 0.85 mg/g, 0.57 ± 0.02 mg/g, 4.38 ± 0.13 mg/g, and 5.50 ± 0.15 mg/g, respectively.

RR Improved Thrombosis in Rats

To determine whether RR exerts an antithrombosis effect, we treated thrombotic rats with three different doses of RR extract. Rats in RR-H, RR-M, and RR-L group were treated with RR extracts at 5.4 g/kg (equivalent to 242.19 ± 4.59 mg/kg catalpol, 3.09 ± 0.11 mg/kg aucubin, 23.65 ± 0.70 mg/kg rehmannioside D, and 29.70 ± 0.81 mg/kg ajugol), 2.7 g/kg (equivalent to 121.10 ± 2.30 mg/kg catalpol, 1.54 ± 0.05 mg/kg aucubin, 11.83 ± 0.35 mg/kg rehmannioside D, and 14.85 ± 0.41 mg/kg ajugol), and 1.35 g/kg (equivalent to 60.55 ± 1.15 mg/kg catalpol, 0.77 ± 0.03 mg/kg aucubin, 5.91 ± 0.18 mg/kg rehmannioside D, and 7.43 ± 0.20 mg/kg ajugol), respectively. Thrombosis in the tail, coagulation function, ET-1/NO, TNF-α, and IL-6 levels were measured. Figure 1A showed that deep red paws, ears, and thrombosis in the tail were observed in the model group, indicating that the model was successfully established. Compared with the model group, the length of thrombosis was shortened after the administration of RR at different dosages. Specifically, the thrombosis length in the RR-L group tended to shorten within 12–48 h ($P > 0.05$). The thrombosis length of the RR-M group was not significantly shortened at 12 h ($P > 0.05$) but decreased at 24 h and 48 h ($P < 0.01$). The thrombosis length was significantly shortened in both the RR-H and AP groups at all observation time ($P < 0.01$). As shown in Figure 1B–E, compared with the control group, plasma prothrombin time (PT, Figure 1B), activated partial thromboplastin time (APTT, Figure 1C), and thrombin time (TT, Figure 1D) were significantly shortened ($P < 0.01$), but fibrinogen (FIB, Figure 1E) was increased ($P < 0.01$) in the model group, indicating that rats in the model group had coagulation dysfunction. Compared with the model group, RR-L prolonged PT, APTT, and TT, and reduced
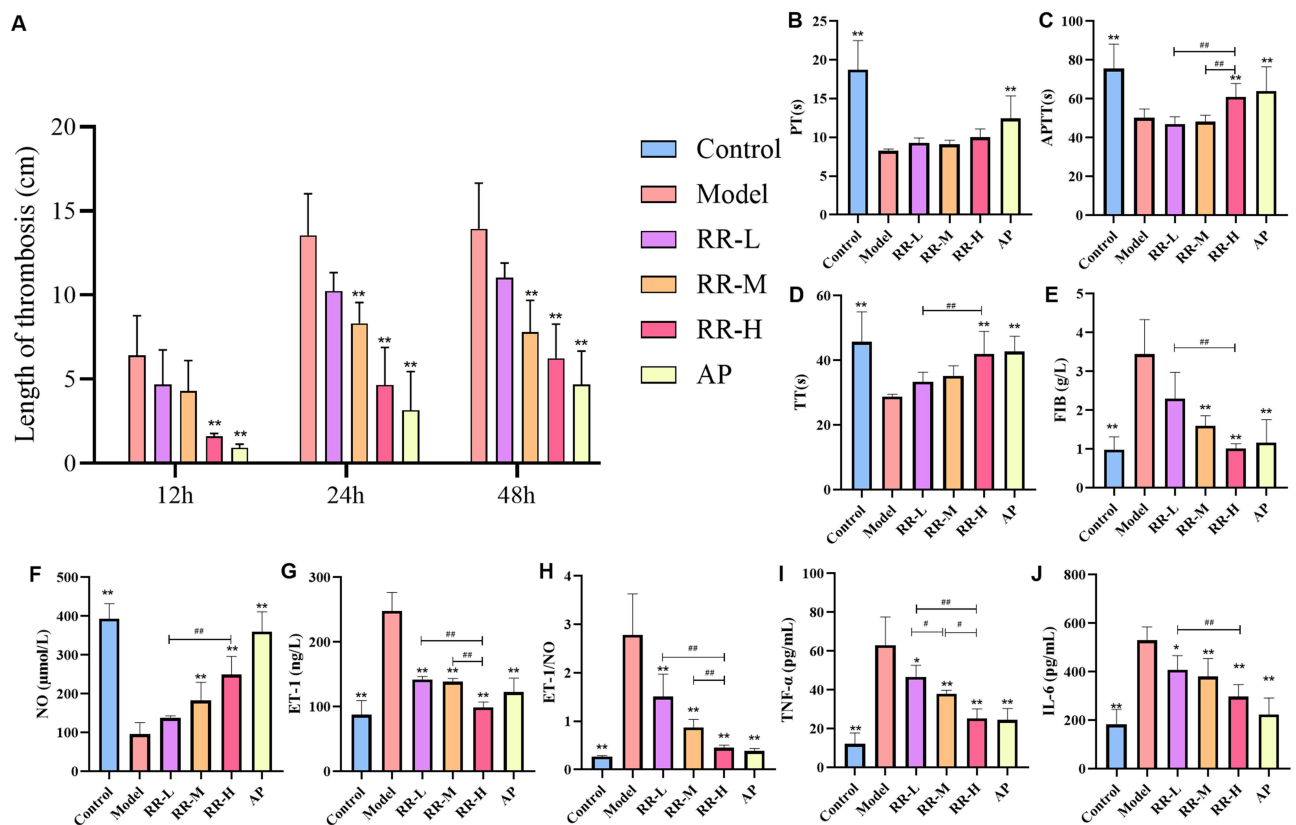

Figure 1 The effects of different dosages of *Rehmanniae Radix* (RR) on the length of thrombosis, coagulation function, and serum biochemical indexes in rats (*n* = 10). (**A**) The length of thrombosis. (**B**) PT. (**C**) APTT. (**D**) TT. (**E**) FIB. (**F**) NO. (**G**) ET-1. (**H**) ET-1/NO. (**I**) TNF-α. (**J**) IL-6. PT, plasma prothrombin time; APTT, activated partial thromboplastin time; TT, thrombin time; FIB, fibrinogen; ET-1, endothelin-1; NO, nitric oxide; TNF-α, tumor necrosis factor-α; IL-6, interleukin-6. *$P < 0.05$, **$P < 0.01$ vs model group; #$P < 0.05$, ##$P < 0.01$ suggested statistical significance compared within groups given with different doses of RR. All data were expressed as mean ± SD.

FIB content ($P > 0.05$), whereas RR-M reduced FIB ($P < 0.01$) and RR-H prolonged APTT and TT and reduced FIB levels ($P < 0.01$), without affecting PT ($P > 0.05$).

The serum levels of NO (Figure 1F), ET-1 (Figure 1G), ET-1/NO (Figure 1H), TNF-α (Figure 1I), and IL-6 (Figure 1J) were determined using an ELISA kit. The results showed the levels of ET-1/NO, TNF-α, and IL-6 were significantly increased in the model group ($P < 0.01$), indicating a disorder in vascular endothelial contractile function and vascular inflammation. Compared with the model group, the levels of ET-1/NO, TNF-α, and IL-6 in all animals treated with different doses of RR were significantly decreased. These results suggested that RR exerted an antithrombotic effect in a dose-dependent manner.

RR Improved Histopathological Damage in Ear and Carotid Artery

Figure 2 showed representative images of HE-stained sections of the ears and carotid arteries, which could reflect thrombus status in the capillaries and damage to the carotid wall. This suggested that the main pathological manifestations in the ears of
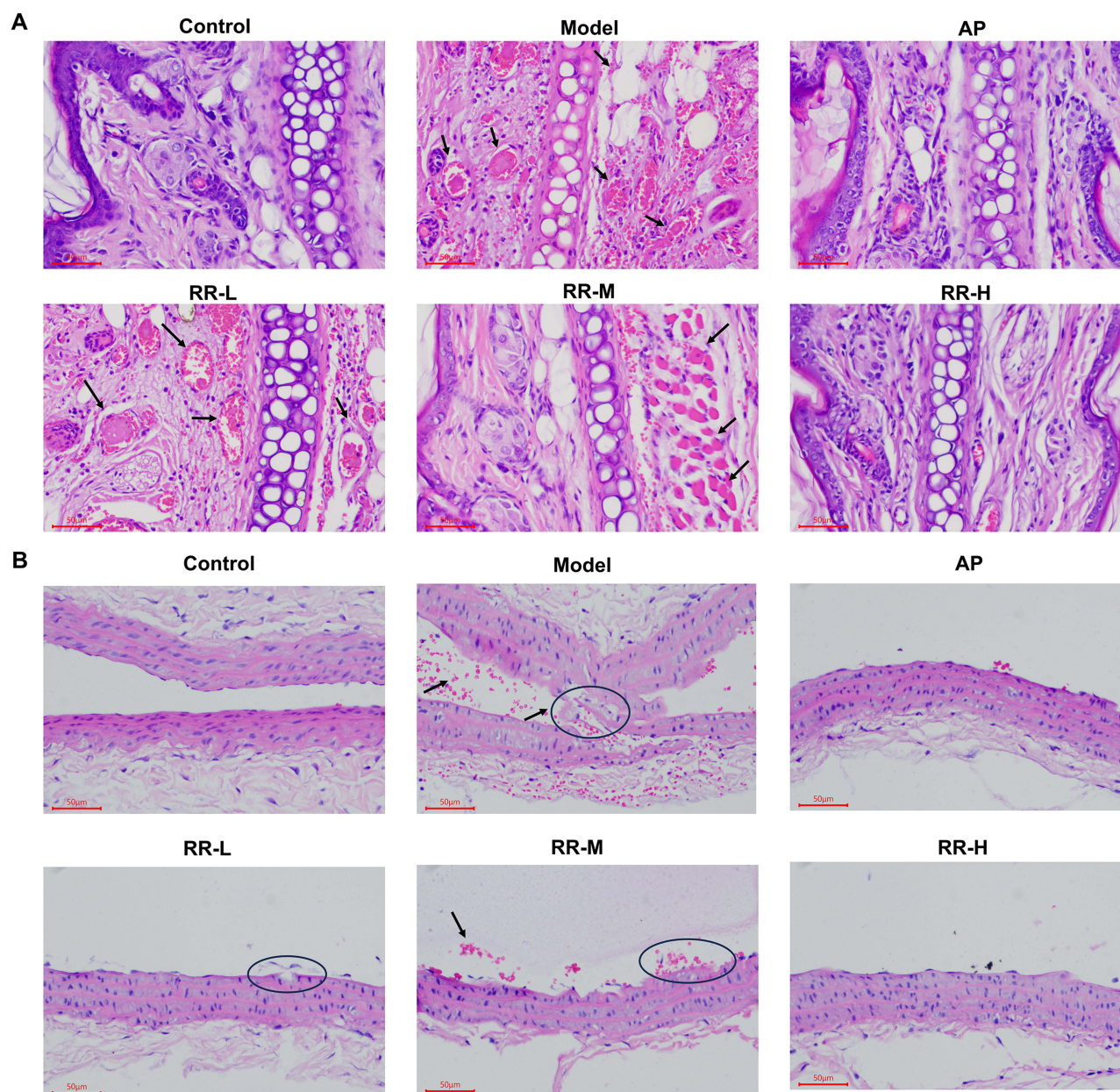

Figure 2 The intervention effects of different dosages of *Rehmanniae Radix* on ear tissues (**A**) and carotid arteries (**B**) in rats with thrombosis (HE, ×200). The arrow indicated the red blood clots, the local fracture of vascular lining, and the shedding of vascular endothelial cells.

rats in the model group were blood capillary dilatation, red blood clots spreading through the veins, membrane endothelial fibrosis, hyperplasia, and inflammatory cell infiltration, all of which are characteristics of thrombosis. However, this damage was relieved by RR (Figure 2A). Moderate congestion and a small amount of inflammatory cell infiltration were observed in the RR-L group. Mild congestion was observed in the RR-M group. No histopathological damage was observed in the RR-H or AP groups.

The effect of RR on thrombi could also be investigated by evaluating carotid vascular endothelial injury. The results showed that the carotid artery endothelial cells were closely packed with a neat, clear outline in the control group, whereas local fracture of the vascular lining was observed in the model group, accompanied by shedding of vascular endothelial cells into the vascular lumen. However, RR treatment prevented endothelial cell shedding and reduced the carotid vascular endothelial injury (Figure 2B). Specifically, local fracture of the vascular lining was observed in the RR-L group, vascular endothelial cells were exfoliated in the RR-M group, and no histopathological damage was observed in the RR-H and AP groups. In general, RR treatment improved histopathological damage to the ears and carotid arteries.

Metabolomics Profiling, Differential Metabolite Identification, and Pathway Analysis

Given the evident antithrombotic bioactivity of RR, a metabolomic study was performed to explore the mechanism underlying its therapeutic effects on thrombosis. PCA was first applied to provide an overview of metabolite modulation by the RR treatment. The obvious aggregation of QC samples in both positive (Figure 3A) and negative (Figure 3B) ion modes indicated good stability of the UPLC Q-TOF/MS system. R^2X and Q^2 which were higher than the recommended value of 0.50 were used to monitor the fitness of the PCA model.[21] It was clear that the metabolic profiling of each group had a better cluster performance in the positive ion mode than in the negative ion mode. In the positive ion mode, there was an obvious separation between the control and model groups, as well as between the model group and different RR groups, indicating that the metabolic status of each group was different. The metabolic profile of thrombotic rats treated with RR-H was closer to that of normal control rats than that of rats in the RR-M and RR-L groups, suggesting that RR-H had a stronger effect on modulating metabolic disorders caused by thrombi than RR-L and RR-M. Although the groups were not completely separated in the negative ion mode, the overall metabolism was still close to that of the control group after the administration of different doses of RR. These results indicated that different doses of RR played a positive role in modulating the metabolic status of thrombosis.

To further identify specific variables among the groups, we performed OPLS-DA between every two groups in both positive (Figure 4) and negative (Figure 5) ion modes. Each OPLS-DA model showed good separation with high R^2Y and Q^2 values, indicating a good explanative ability of sample classification information and cross-validated predictive capability. Moreover, a permutation test with 200 iterations verified that the models were nonoverfitted and reliable. The differential metabolites between the RR and model groups were screened using an S-plot. Based on VIP > 1.0, |p(corr)| > 0.5, and $P < 0.05$,[22] 13 metabolites were considered as key differential metabolites (Table 1).
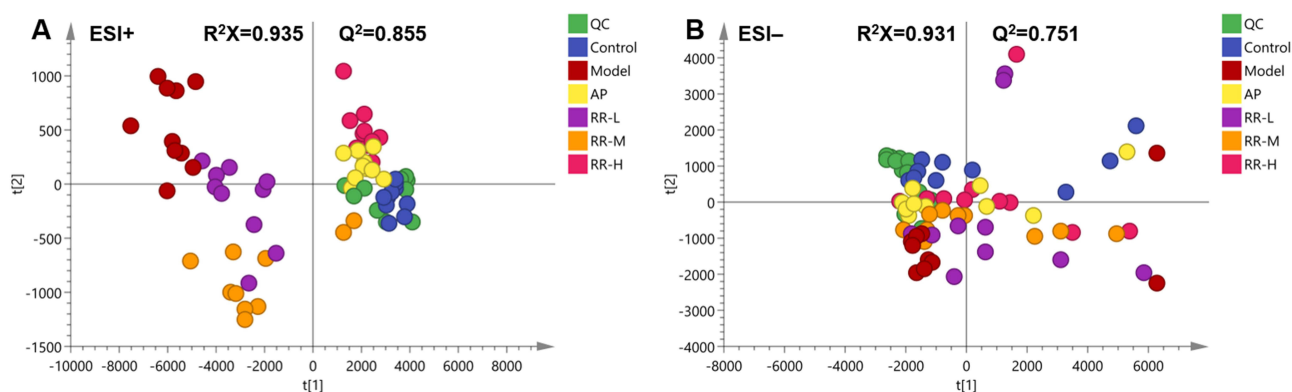

Figure 3 Principal component analysis score plot of serum metabolomics analysis (n = 10). (**A**) positive ion mode. (**B**) negative ion mode. ESI, electrospray ionization.
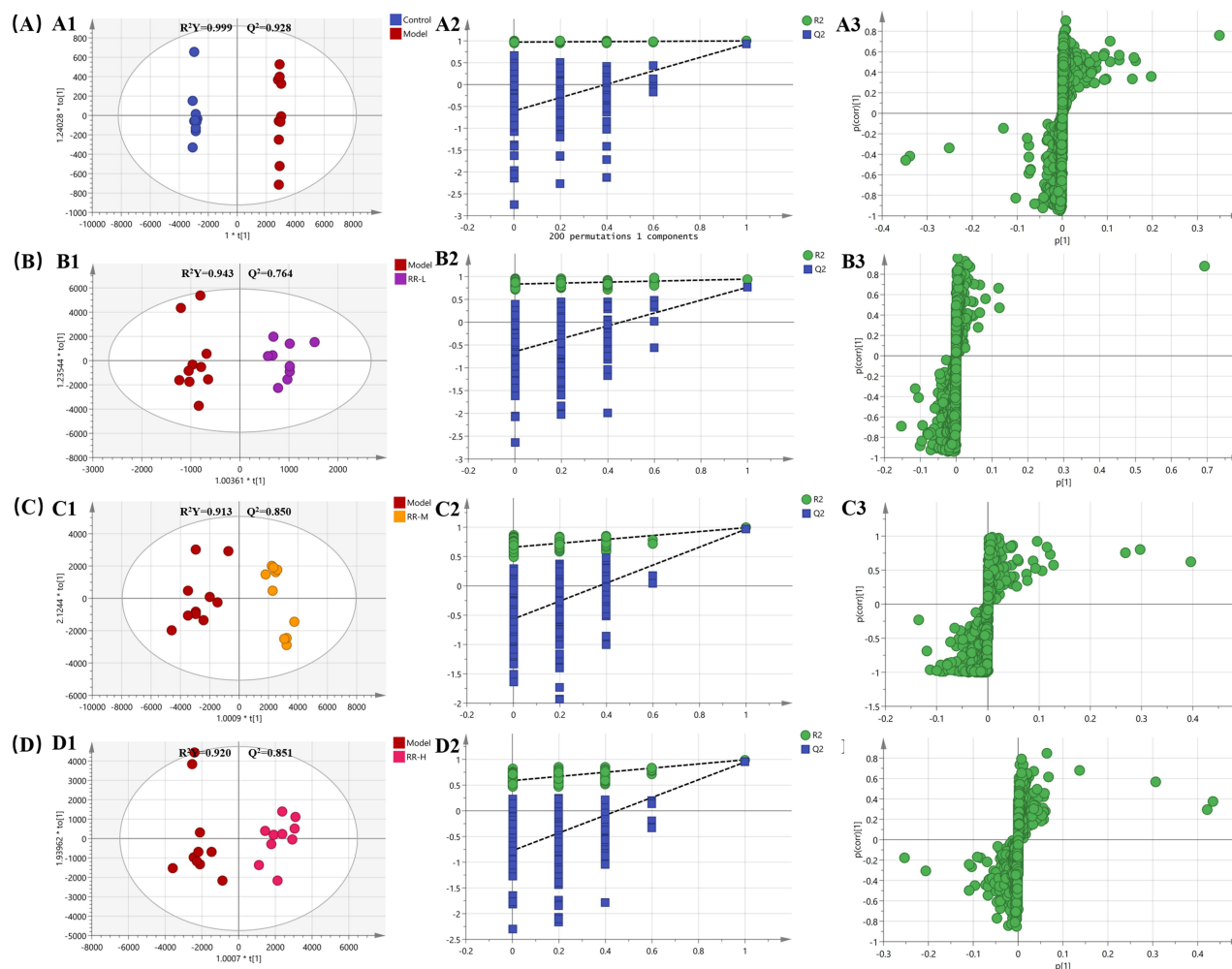
Figure 4 Orthogonal partial least-squares discrimination analysis. Score plot (A1, B1, C1 and D1), 200 iteration replacement tests (A2, B2, C2 and D2), and S-plot curve (A3, B3, C3 and D3) in positive ion mode (*n* = 10). (**A**) Control vs Model. (**B**) Model vs RR-L. (**C**) Model vs RR-M. (**D**) Model vs RR-H. RR, *Rehmanniae Radix.*.

To explore the effect of RR on the metabolism of thrombotic rats, the peak area was used as the reference to observe the relative content changes of the 13 thrombosis markers in the different RR groups (Figure 6A–M). It is important to highlight that the therapeutic effects of TCM stem from their influence on the dynamic balance of multiple metabolites. Therefore, alterations in a single metabolite do not adequately represent the overall therapeutic effect. The results showed that UDP-N-acetylmuramoyl-L-alanyl-D-glutamate, dichloroacetate and bullatanocin of RR groups did not directly modify the serum levels of metabolites in thrombotic mice. Hierarchical clustering analysis of the metabolites in each group was performed using bioinformatics (https://www.bioinformatics.com.cn/), in which the overall similarity and differences between groups could be intuitively observed (Figure 6N). With an increase in the dose of RR, the metabolite expression was closer to that of the control group. The RR-H group showed a better antithrombotic effect, with metabolic characteristics similar to those of the control group.

To explore the metabolic pathways related to RR treatment in thrombosis rats, we imported these differential metabolites into MetaboAnalyst 5.0. As shown in Table 2 and Figure 6O, three pathways with impact > 0.1 and –log (*P*) > 1 were significantly affected, including arachidonic acid metabolism, sphingolipid metabolism, and glycerophospholipid metabolism.
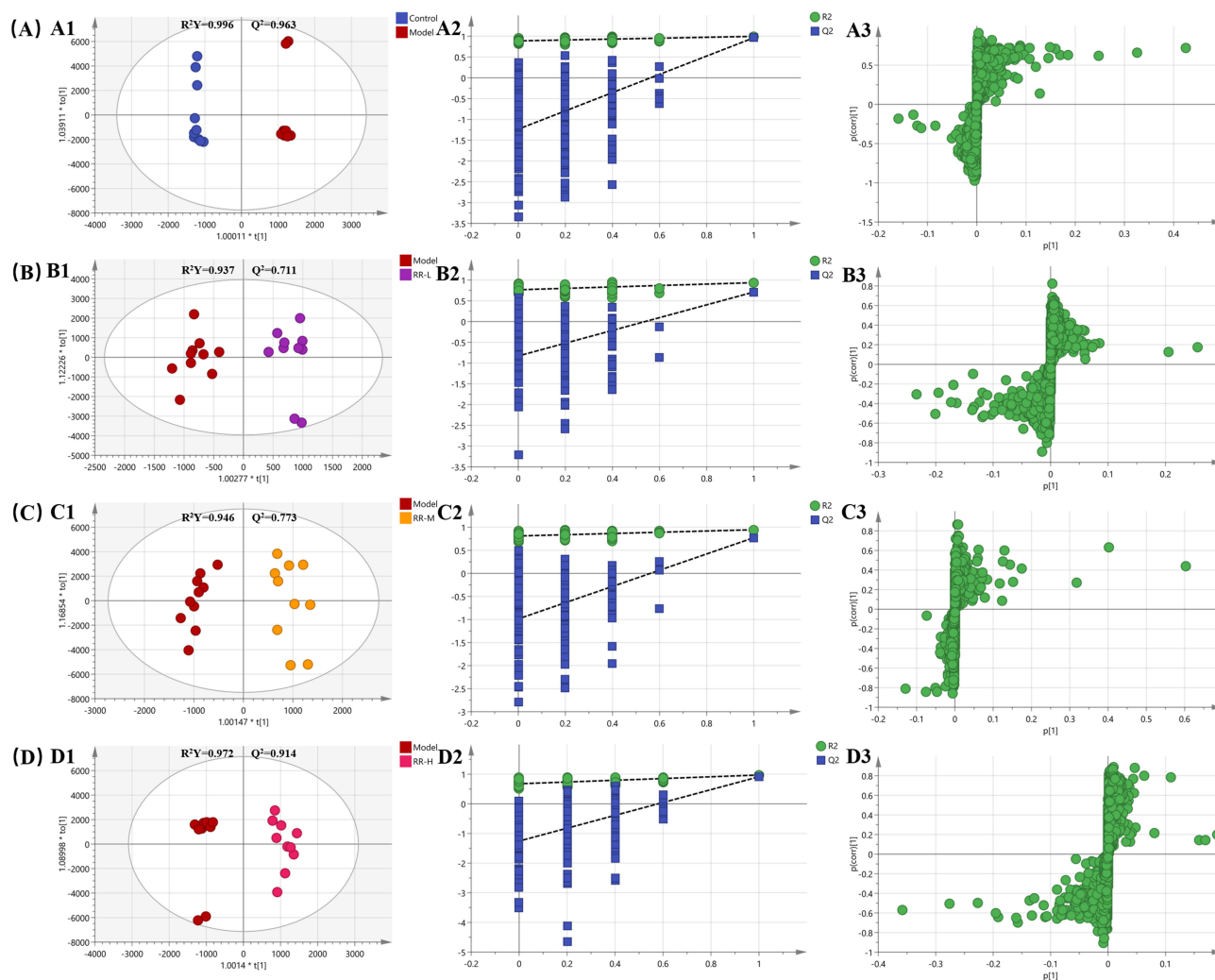
Figure 5 Orthogonal partial least-squares discrimination analysis. Score plot (A1, B1, C1 and D1), 200 iteration replacement tests (A2, B2, C2 and D2), and S-plot curve (A3, B3, C3 and D3) in negative ion mode (*n* = 10). (**A**) Control vs Model. (**B**) Model vs RR-L. (**C**) Model vs RR-M. (**D**) Model vs RR-H. RR, *Rehmanniae Radix.*.

Network Pharmacology Study

A network pharmacology study was conducted to explore the material basis and mechanism of RR in thrombosis. Twenty-four eligible RR compounds were identified from public databases (Table S1). In addition, 362 targets of these compounds were obtained from TCMSP, SwissTargetPrediction, and BATMAN-TCM databases. Using the GeneCards database, 954 thrombosis-related targets were identified. The 97 overlapping targets of the disease and drug were considered potential targets for RR in the treatment of thrombosis (Figure 7A and Table S2). To assess the biological characteristics of therapeutic targets, GO and KEGG analyses were performed using the DAVID database. In KEGG enrichment analysis (Figure 7B), the pathways that were significantly affected were lipid and atherosclerosis, pathways in cancer, and proteoglycans in cancer. GO enrichment analysis was used to identify underlying biological processes, cellular components, and molecular functions. The top terms were cytokine-mediated signaling pathways and positive regulation of the ERK1 and ERK2 cascades (Figure 7C). The compounds in RR, therapeutic targets, and top 20 KEGG pathways were imported into STRING and Cytoscape to build a compound-target-pathway network (Figure 7D), which could intuitively reflect the relationships of compounds, targets, and metabolic pathways. A total of 136 nodes and 1485 edges were generated in the network. Ferulic acid methyl ester, catalpol, rhmaionoside C, and methyl 4-hydroxycinnamate exhibited high degrees in the network. Thus, these compounds might be key compounds in RR treating thrombosis

Table 1 Basic Characteristics of Thrombosis Biomarkers

| Mode	No.	Metabolite	Formula	Accurate Mass (m/z)		Error (ppm)	MS Fragments	Retention Time (min)	KEGG ID
				Predicted	Measured				
ESI⁺	M1	PC (20:2(11Z, 14Z)/14:0)	$C_{42}H_{81}NO_8P$	759.5778	759.5839	8	740.5568, 291.2673, 211.2056	14.366	C00157
	M2	Arachidonic acid	$C_{20}H_{32}O_2$	305.248	305.2510	10	303.2332, 259.2433	14.133	C00219
	M3	Docosahexaenoic acid	$C_{22}H_{32}O_2$	329.248	329.2509	9	329.2466, 311.2368, 269.2263, 187.1466, 163.1472	13.852	C06429
	M4	LysoPC (18:0)	$C_{26}H_{55}NO_7P$	525.3794	525.3826	6	526.3775, 184.0733, 104.1062	11.949	C04230
	M5	Solanidine	$C_{27}H_{43}NO$	398.3423	398.3405	−5	380.3323, 352.3023, 126.1258	15.09	C06543
	M6	UDP-N-acetylmuramoyl-L-alanyl-D-glutamate	$C_{28}H_{43}N_5O_{23}P_2$	880.1902	880.1835	−8	219.0923, 146. 0476, 113.0375	5.702	C00692
	M7	Dichloroacetate	$C_2H_2Cl_2O_2$	128.951	128.9516	5	117.0354, 89.0423, 73.0123	18.436	C11149
	M8	Sphinganine	$C_{18}H_{39}NO_2$	302.3059	302.3054	−2	302.7698, 284.6523, 266.5662	14.133	C00836
	M9	Sphingosine-1-phosphate	$C_{18}H_{38}NO_5P$	380.2565	380.2575	3	362.2465, 264.2708, 247.2422, 93.0723	7.429	C06124
	M10	Bullatanocin	$C_{37}H_{66}O_8$	639.4835	639.4786	−8	621.4732, 603.4638, 97.0290	15.564	C08505
	M11	Thromboxane A2	$C_{20}H_{32}O_5$	353.2328	353.2355	8	335.2211, 317.2123, 241.1368	11.325	C02198
ESI⁻	M12	PI (20:2(11Z, 14Z)/16:0)	$C_{45}H_{83}O_{13}P$	861.5493	861.5530	4	253.0242, 237.2253, 78.9584	18.226	C00626
	M13	Taurocholic acid	$C_{26}H_{45}NO_7S$	514.2838	514.2804	−7	495.3132, 352.6213	6.139	C05122
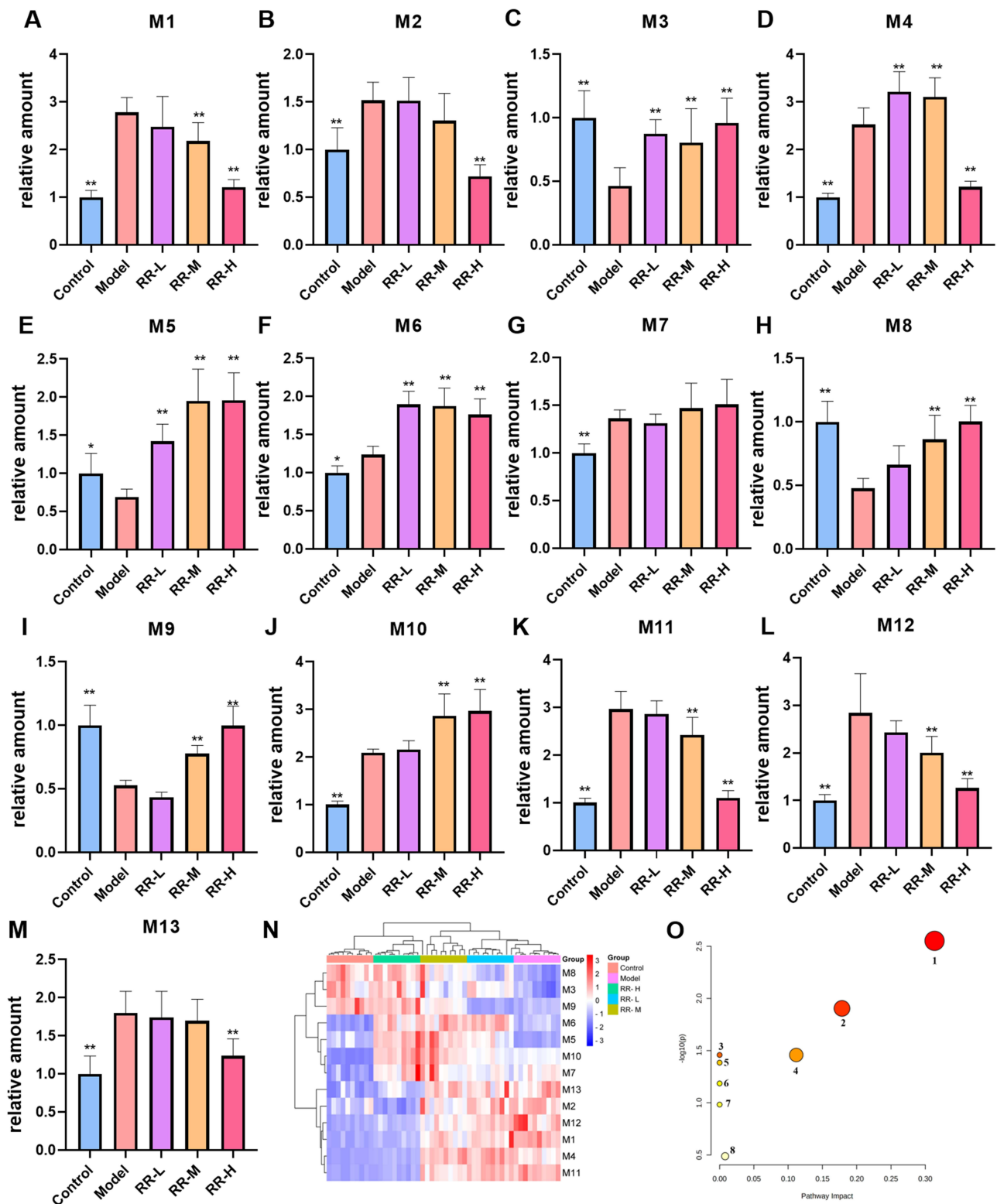
Figure 6 Relative content changes of thrombosis markers and the dominant metabolic pathway after *Rehmanniae Radix* treatment (*n* = 10). (**A**) M1, PC (20:2(11Z, 14Z)/14:0). (**B**) M2, Arachidonic acid. (**C**) M3, Docosahexaenoic acid. (**D**) M4, LysoPC (18:0). (**E**) M5, Solanidine. (**F**) M6, UDP-N-acetylmuramoyl-L-alanyl-D-glutamate. (**G**) M7, Dichloroacetate. (**H**) M8, Sphinganine. (**I**) M9, Sphingosine-1-phosphate. (**J**) M10, Bullatanocin. (**K**) M11, Thromboxane A2. (**L**) M12, PI (20:2(11Z, 14Z)/16:0). (**M**) M13, Taurocholic acid. (**N**) Heat map of metabolite clustering. (**O**) The dominant metabolic pathway. *$P<0.05$ vs Model, **$P<0.01$ vs Model. All data are expressed as mean ± SD.

Table 2 Ingenuity Pathway Analysis

No.	Pathway	Match Status	p	-log(p)	Holm p	FDR	Impact
1	Arachidonic acid metabolism	3/36	0.0028068	2.5518	0.23577	0.23577	0.3135
2	Sphingolipid metabolism	2/21	0.012469	1.9042	1	0.52368	0.1785
3	Biosynthesis of unsaturated fatty acids	2/36	0.034843	1.4579	1	0.69368	0
4	Glycerophospholipid metabolism	2/36	0.034843	1.4579	1	0.69368	0.11182
5	Linoleic acid metabolism	1/5	0.04129	1.3842	1	0.69368	0
6	Taurine and hypotaurine metabolism	1/8	0.065303	1.1851	1	0.91424	0
7	Alpha-Linolenic acid metabolism	1/13	0.10409	0.98257	1	1	0
8	Primary bile acid biosynthesis	1/46	0.3251	0.48798	1	1	0.00805

(Table S3). Moreover, the metabolite-target network was built using MBrole and Cytoscape, with 291 nodes and 437 edges, indicating that the differential metabolites were associated with multiple targets (Figure 7E).

Integrated Analysis of Metabolomics and Network Pharmacology Study

We constructed an interaction network based on metabolomics and network pharmacology studies to obtain a comprehensive view of the mechanisms of RR in thrombosis. The combination of the compound-target-pathway network and metabolite-target network highlighted four hub targets: PLA2G2A, CYP2C9, PTGS1, and ALOX5. After removing the nodes that were not associated with the above four hub genes, a compound-target-metabolite network was obtained (Figure 7F). The key metabolites were arachidonic acid (AA) and PC (20:2(11Z, 14Z)/14:0). The affected pathways were arachidonic acid and glycerophospholipid metabolism, consistent with the main pathways discovered in the metabolomics study. The active compounds were catalpol, ferulic acid methyl ester, methyl 4-hydroxycinnamate, and rehmaionoside C, which might play essential roles in the therapeutic effect of RR against thrombosis.

Molecular Docking

Molecular docking was used to validate the possibility of interactions between the key targets and related compounds. The binding energies of the compounds and targets were listed in Table 3. The optimal docking conformation was visualized using the PyMoL software. The catalpol formed hydrogen bonds with LYS-62, ASN-114, GLY-22, and CYS-28 of PLA2G2A (Figure 8A). The ferulic acid methyl ester formed hydrogen bonds with ASN-554 and GLU-557 in ALOX5 (Figure 8B). Figure 8C showed that methyl 4-hydroxycinnamate formed hydrogen bonds with TYR-558 and PHE-555 in ALOX5. Rehmaionoside C formed hydrogen bonds with ARG-246, THR-249, and GLU-250 in ALOX5 (Figure 8D). Figure 8E showed that methyl 4-hydroxycinnamate formed hydrogen bonds with HIS-43, LYS-468, and GLN-461 in PTGS1. Figure 8F showed that hydrogen bonds were formed between catalpol and GLN-484, HPE-482, and ASP-468 of CYP2C9.

A binding energy less than 0 kcal/mol indicates effective docking, and less than −5 kcal/mol indicates high affinities.[23,24] The molecular docking results showed that catalpol-PLA2G2A, methyl 4-hydroxycinnamate-PTGS1, ferulic acid methyl ester-ALOX5, and methyl 4-hydroxycinnamate-ALOX5 binding energies were less than −5 kcal/mol, indicating that the three compounds had a high affinity for their core proteins. Therefore, we predicted that catalpol, ferulic acid methyl ester, and methyl 4-hydroxycinnamate might play critical roles in the treatment of thrombosis by RR via interactions with PLA2G2A, PTGS1, and ALOX5.

Discussion

Currently, thrombosis is an incredible burden to human health. Therefore, it is necessary to discover novel therapeutic approaches and clarify their underlying mechanisms. In this study, the antithrombotic effects of different RR doses were verified in carrageenan-induced thrombotic rats. It was observed that a high dose of RR had more promising antithrombotic bioactivity. The strategy of combining metabolomics and network pharmacology was followed to elucidate the potential antithrombosis mechanism of RR. We identified 13 significant metabolites of RR against thrombosis in the
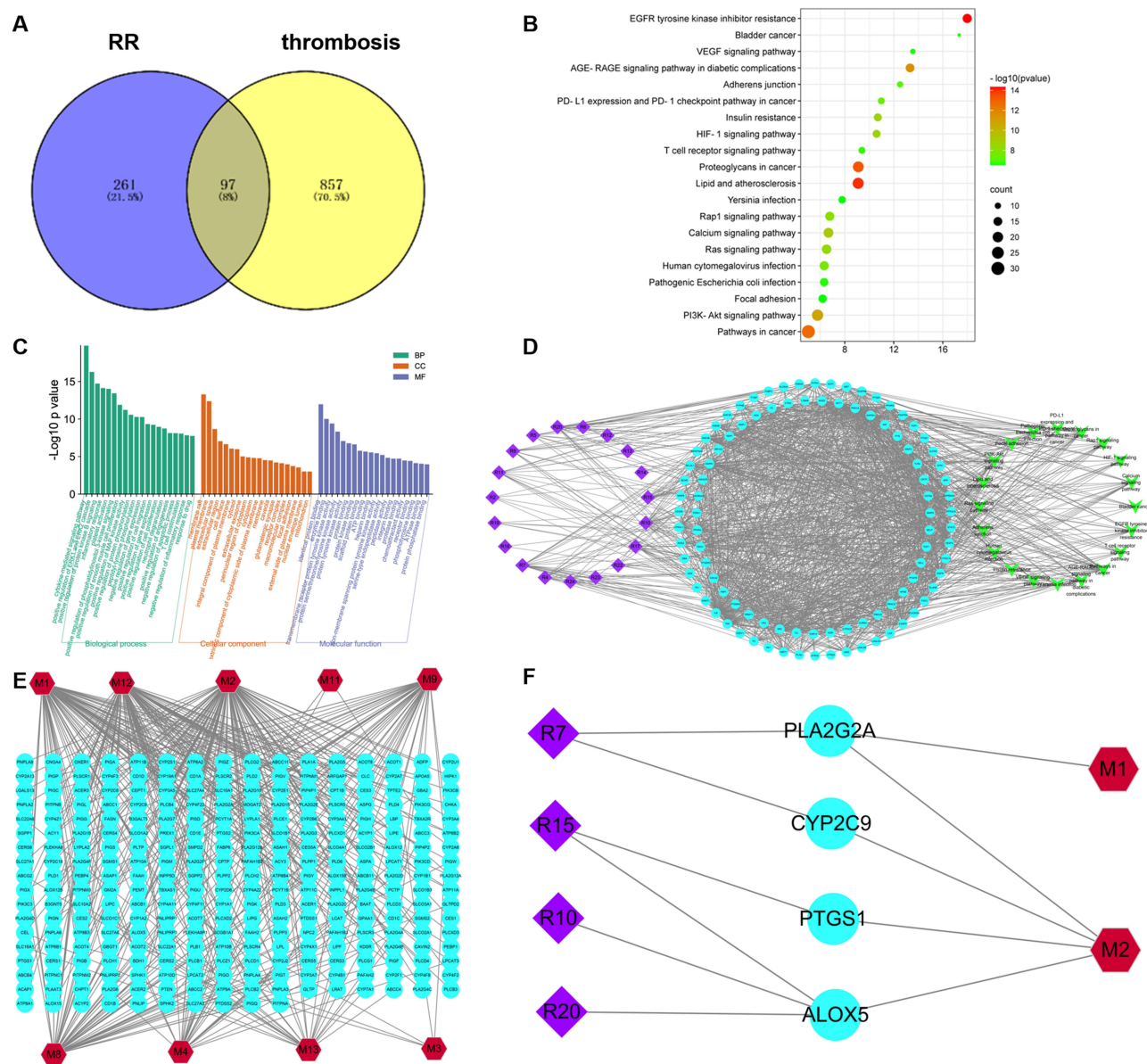
Figure 7 Network pharmacology results of *Rehmanniae Radix* (RR) against thrombosis. (**A**) The overlapped targets of RR and thrombosis. (**B**) KEGG pathways enrichment. (**C**) GO terms enrichment. (**D**) compound-target-pathway network. (**E**) metabolite-target network. (**F**) compound-target-metabolite network. The purple diamond was the compounds of RR; the blue ellipse was the target; the green V was the pathway; the red hexagon was the metabolite. R7, catalpol; R10, ferulic acid methyl ester; R15, methyl 4-hydroxycinnamate; R20, rehmaionoside C; M1, PC (20:2(11Z, 14Z)/14:0); M2, arachidonic acid.

serum, as well as their related metabolic pathways. A network pharmacology study was conducted to predict the active compounds, targets, and signaling pathways of RR against thrombosis. By combining metabolomics with network pharmacology, we identified four key targets (PLA2G2A, CYP2C9, PTGS1, and ALOX5), two key metabolites (PC (20:2(11Z, 14Z)/14:0) and arachidonic acid), and four related compounds (catalpol, ferulic acid methyl ester, methyl 4-hydroxycinnamate, and rehmaionoside C). Molecular docking was used to validate the possibility of interactions between the key targets and related compounds. This strategy provides a reference for screening key compounds, major metabolites, and critical targets for the study of other natural products.

Among the predicted active compounds, catalpol, an important iridoid glycoside quality marker isolated from RR, has been shown to be the main component responsible for the antithrombotic activity of RR. Catalpol exerted synergistic antithrombotic effects by inhibiting the expression of inflammatory factors and regulating the balance of the fibrinolysis system.[7] In addition, catalpol is able to treat thrombotic diseases, such as ischemic stroke and ischemia/reperfusion

Table 3 Molecular Docking Results of Key Targets with Related Compounds

Targets	Compounds	Binding Energy (kcal/mol)
PLA2G2A	Catalpol	−5.12
ALOX5	Ferulic acid methyl ester	−5.94
ALOX5	Methyl 4-hydroxycinnamate	−5.54
ALOX5	Rehmaionoside C	−2.82
PTGS1	Methyl 4-hydroxycinnamate	−5.62
CYP2C9	Catalpol	−3.39

injury.[25–27] Catalpol could regulate RhoA/ROCK-2 signaling pathway and up-regulate tight junction protein to inhibit LPS-induced blood-brain barrier permeability disorder in thrombosis.[28] The main material basis of the antithrombotic activities of RR is regarded as oligosaccharide and iridoid glycosides components.[7] These findings indicate that it is worthy to further explore the therapeutic effect of catalpol on thrombosis. In addition, according to the theory of TCM, RR was widely used in the syndrome of blood deficiency and blood stasis before the Song Dynasty, with a dosage higher than that prescribed by the Chinese Pharmacopoeia.[5] In this study, the dose in the RR-L group was converted from the recommended dosage in the Chinese Pharmacopoeia, and the doses in the RR-M and RR-H groups were set to explore the antithrombotic effect of RR and explain the relationship between the activity and the dose, which completely simulated clinical practice and followed the requirements of Pharmacopoeia.
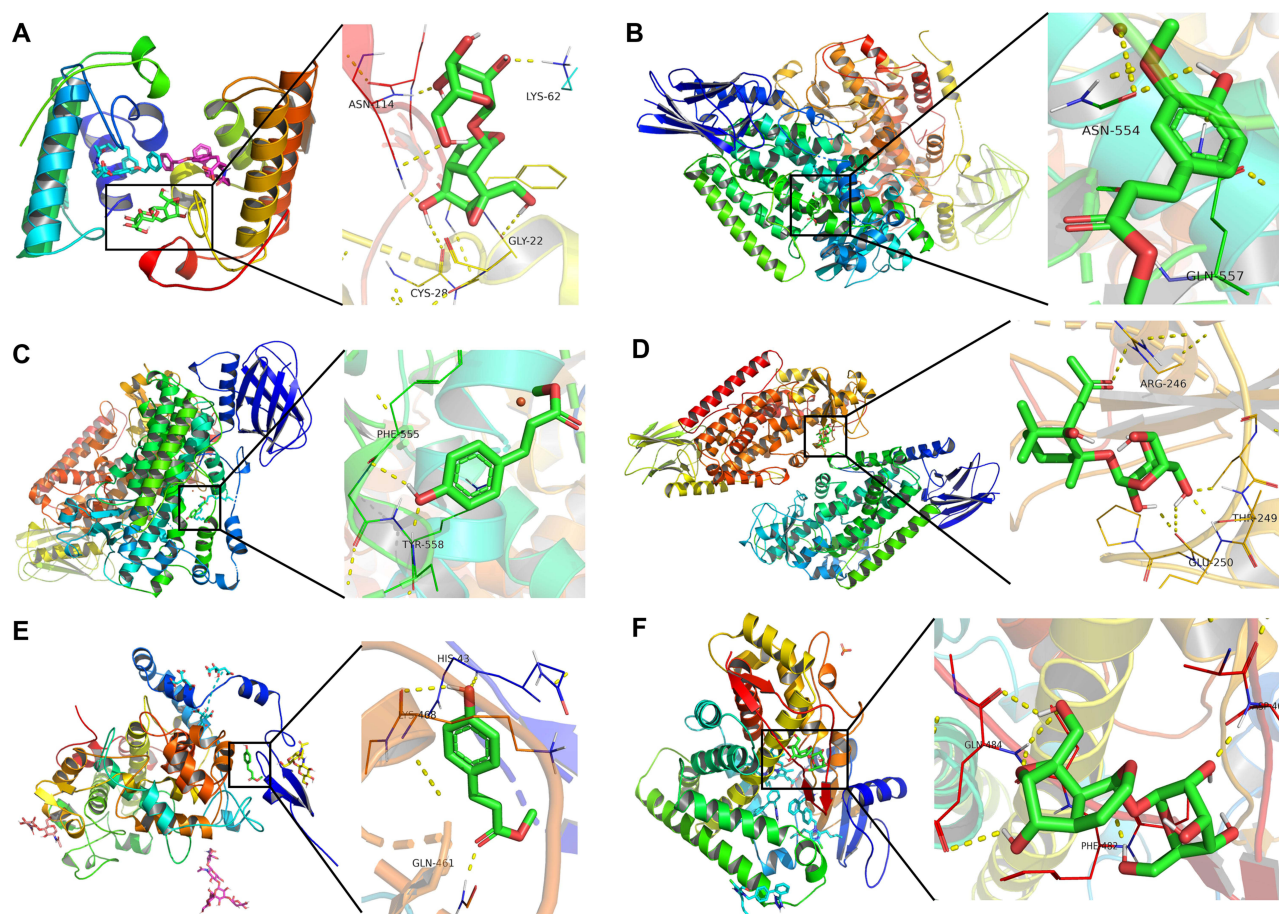

Figure 8 Three-dimension interaction diagram of molecular docking results. (**A**) catalpol and PLA2G2A. (**B**) ferulic acid methyl ester and ALOX5. (**C**) methyl 4-hydroxycinnamate and ALOX5. (**D**) rehmaionoside C and ALOX5. (**E**)methyl 4-hydroxycinnamate and PTGS1. (**F**) catalpol and CYP2C9.

In lipid metabolism, glycerophospholipids produce lysophospholipids and free fatty acids, including AA and DHA, catalyzed by phospholipase A2, which controls the initial rate-limiting step of the biosynthetic cascade.[29] The increased PC level could accelerate the formation of thrombin and promote blood coagulation by binding with coagulation factors, demonstrating a positive correlation between plasma PC level and cardiovascular disease mortality.[30] LysoPCs and AA hydrolyzed from PCs have proinflammatory and prothrombotic activity, interfering vascular endothelial function.[31] Phospholipase A2 is strongly related to lipid degradation in inflammation, antibacterial defense, antithrombotic formation, apoptotic cell clearance, ischemic injury, and allergic reaction, in which especially secretory phospholipase A2 group IIA (encoded by the PLA2G2A) overexpresses in inflammation-related and cardiovascular diseases, thereby increasing AA release.[32–34] Catalyzed by prostaglandin G/H synthases (encoded by the PTGS1 or PTGS2), cytochrome P450 enzymes, or lipid oxygenase (encoded by the ALOX5 or ALOX15), AA can subsequently transform into a series of AA derivatives including thromboxane A2 (TXA2), leukotrienes, and several prostaglandins with multiple functions.[35] Among them, TXA2 is regarded as an important marker of thrombotic diseases, due to its strong ability of constricting blood vessels and promoting platelet aggregation.[36] In the study, the level of PC (20:2(11Z, 14Z)/14:0), AA, LysoPC (18:0), and TXA2 in serum of rats with thrombosis increased significantly. We speculated that the cell biofilm was seriously damaged in rats with thrombosis, which resulted in the accumulation of glycerophospholipids and increased inflammatory conditions in the blood, thus promoting coagulation. After RR administration, the levels of glycerophospholipids, AA, and TXA2 decreased, indicating that RR suppressed lipid degradation. It is also speculated that the binding affinities of catalpol, methyl 4-hydroxycinnamate, and ferulic acid methyl ester in RR might downregulate the expression of PLA2G2A, PTGS1, and ALOX5 to inhibit lipid degradation and relieve thrombosis and inflammation. The key role of these enzymes in lipid metabolism has led to the development of enzyme-targeted therapies. For example, the administration of aspirin, a well-known nonsteroidal anti-inflammatory drug, is an effective preventive therapy among patients at risk of developing or suffering from CVD, due to its inhibiting function by acetylation of the platelet PTGS1 to play an antithrombotic action.[37] Danshen (Salvia miltiorrhiza), a beneficial Chinese medicine on blood stasis syndrome, activates PLA2G1B and PLA2G2A to resolve the disturbance of glycerophospholipid metabolism.[38] Gualou (Trichosanthes kirilowii Maxim)-Xiebai (Allium macrostemon Bunge) is a well-known herb pair, suppressing the inflammatory target levels of ALOX5 and PTGS2 to against atherosclerosis.[39] Luteolin, a natural ingredient from several herbs, restrains the activation of ALOX5, ALOX12, and ALOX15 in lipoxygenase pathway to treat oxygen-glucose deprivation/reperfusion injury.[40] These findings highlight the prospective therapeutic development targeting these key enzymes to treat thrombosis.

Conclusion

In this study, 13 metabolites related to lipid metabolism were identified by metabolomics. Combined with the potential targets obtained by network pharmacology, four shared targets were considered potential targets: PLA2G2A, CYP2C9, PTGS1, and ALOX5. Catalpol, ferulic acid methyl ester, and methyl 4-hydroxycinnamate might be the key compounds responsible for the antithrombotic bioactivity of RR via interactions with PLA2G2A, PTGS1, and ALOX5. Further in vitro and in vivo studies are required to validate these findings. Generally, the strategy of integrating metabolomics and network pharmacology study could be an effective approach for clarifying the systemic mechanism of natural products in the treatment of diseases.

Funding

Disclosure

The authors declare that they have no competing interests in this work.

References

1. Stark K, Massberg S. Interplay between inflammation and thrombosis in cardiovascular pathology. *Nat Rev Cardiol*. 2021;18(9):666–682. doi:10.1038/s41569-021-00552-1

2. Asada Y, Yamashita A, Sato Y, et al. Thrombus formation and propagation in the onset of cardiovascular events. *J Atheroscler Thromb*. 2018;25 (8):653–664. doi:10.5551/jat.RV17022

3. Wijeyeratne YD, Heptinstall S. Anti-platelet therapy: ADP receptor antagonists. *Br J Clin Pharmacol*. 2011;72(4):647–657. doi:10.1111/j.1365-2125.2011.03999.x

4. Zhao Y, Nie S, Yi M, et al. UPLC-QTOF/MS-based metabolomics analysis of plasma reveals an effect of Xue-Fu-Zhu-Yu capsules on blood-stasis syndrome in CHD rats. *J Ethnopharmacol*. 2019;241:111908. doi:10.1016/j.jep.2019.111908

5. Wu MQ, Peng W, Zhou X, et al. Research progress on materia medica and clinical application about efficacy of activating blood and resolving stasis of *Rehmanniae Radix*. *Chin J Tradit Chin Med Pharm*. 2020;35:3553–3556.

6. Gong PY, Tian YS, Guo YJ, et al. Comparisons of antithrombosis, hematopoietic effects and chemical profiles of dried and rice wine-processed *Rehmanniae Radix* extracts. *J Ethnopharmacol*. 2019;231:394–402. doi:10.1016/j.jep.2018.10.025

7. Gong PY, Guo YJ, Tian YS, et al. Reverse tracing anti-thrombotic active ingredients from dried Rehmannia Radix based on multidimensional spectrum-effect relationship analysis of steaming and drying for nine cycles. *J Ethnopharmacol*. 2021;276:114177. doi:10.1016/j.jep.2021.114177

8. Guo W, Wang Y, Fan M, et al. Integrating metabolomics and network pharmacology to explore the protective effect of gross saponins of Tribulus terrestris L. fruit against ischemic stroke in rat. *J Ethnopharmacol*. 2020;263:113202. doi:10.1016/j.jep.2020.113202

9. Li X, Wei S, Niu S, et al. Network pharmacology prediction and molecular docking-based strategy to explore the potential mechanism of Huanglian Jiedu Decoction against sepsis. *Comput Biol Med*. 2022;144:105389. doi:10.1016/j.compbiomed.2022.105389

10. Yuan Z, Pan Y, Leng T, et al. Progress and prospects of research ideas and methods in the network pharmacology of traditional Chinese medicine. *J Pharm Pharm Sci*. 2022;25:218–226. doi:10.18433/jpps32911

11. Chinese Pharmacopoeia Commission. *Pharmacopoeia of the People's Republic of China*. 2020 ed. Beijing: China Medical Science Press; 2020.

12. Ma N, Liu XW, Yang YJ, et al. Preventive effect of aspirin eugenol ester on thrombosis in κ-carrageenan-induced rat tail thrombosis model. *PLoS One*. 2015;10(7):e0133125. doi:10.1371/journal.pone.0133125

13. Su L, Mao J, Hao M, et al. Integrated plasma and bile metabolomics based on an UHPLC-Q/TOF-MS and network pharmacology approach to explore the potential mechanism of Schisandra chinensis-protection from acute alcoholic liver injury. *Front Pharmacol*. 2020;10:1543. doi:10.3389/fphar.2019.01543

14. Feldman AT, Wolfe D. Tissue processing and hematoxylin and eosin staining. *Methods Mol Biol*. 2014;1180:31–43.

15. Du Y, Fan P, Zou L, et al. Serum metabolomics study of papillary thyroid carcinoma based on HPLC-Q-TOF-MS/MS. *Front Cell Dev Biol*. 2021;9:593510. doi:10.3389/fcell.2021.593510

16. Wang J, Wang Y, Zeng Y, Huang D. Feature selection approaches identify potential plasma metabolites in postmenopausal osteoporosis patients. *Metabolomics*. 2022;18(11):86. doi:10.1007/s11306-022-01937-0

17. Howell A, Yaros C. Downloading and analysis of metabolomic and lipidomic data from metabolomics workbench using MetaboAnalyst 5.0. *Methods Mol Biol*. 2023;2625:313–321.

18. Liu H, Cao M, Jin Y, et al. Network pharmacology and experimental validation to elucidate the pharmacological mechanisms of Bushen Huashi decoction against kidney stones. *Front Endocrinol*. 2023;14:1031895. doi:10.3389/fendo.2023.1031895

19. Ru J, Li P, Wang J, et al. TCMSP: a database of systems pharmacology for drug discovery from herbal medicines. *J Cheminform*. 2014;6:13. doi:10.1186/1758-2946-6-13

20. Mo CL, Li J, Wang JZ, et al. Applicability of a zebrafish thrombosis model in screening active ingredients of traditional Chinese medicine. *Shand Sci*. 2021;34(4):52–59.

21. Abdelrazig S, Safo L, Rance GA, et al. Metabolic characterisation of Magnetospirillum gryphiswaldense MSR-1 using LC-MS-based metabolite profiling. *RSC Adv*. 2020;10(54):32548–32560. doi:10.1039/D0RA05326K

22. Li L, Cui H, Zhang Y, et al. Baicalin ameliorates multidrug-resistant Pseudomonas aeruginosa induced pulmonary inflammation in rat via arginine biosynthesis. *Biomed Pharmacother*. 2023;162:114660. doi:10.1016/j.biopha.2023.114660

23. Shamsol Azman ANS, Tan JJ, Abdullah MNH, et al. Network pharmacology and molecular docking analysis of active compounds in Tualang honey against atherosclerosis. *Foods*. 2023;12(9):1779. doi:10.3390/foods12091779

24. Lu X, Zheng Y, Wen F, et al. Study of the active ingredients and mechanism of Sparganii rhizoma in gastric cancer based on HPLC-Q-TOF-MS/MS and network pharmacology. *Sci Rep*. 2021;11(1):1905. doi:10.1038/s41598-021-81485-0

25. Zhu HF, Wan D, Luo Y, et al. Catalpol increases brain angiogenesis and up-regulates VEGF and EPO in the rat after permanent middle cerebral artery occlusion. *Int J Biol Sci*. 2010;6:443–453. doi:10.7150/ijbs.6.443

26. Dong W, Xian Y, Yuan W, et al. Catalpol stimulates VEGF production via the JAK2/STAT3 pathway to improve angiogenesis in rats' stroke model. *J Ethnopharmacol*. 2016;191:169–179. doi:10.1016/j.jep.2016.06.030

27. Liu YR, Li PW, Suo JJ, et al. Catalpol provides protective effects against cerebral ischaemia/reperfusion injury in gerbils. *J Pharm Pharmacol*. 2014;66:1265–1270. doi:10.1111/jphp.12261

28. Feng S, Zou L, Wang H, et al. RhoA/ROCK-2 pathway inhibition and tight junction protein upregulation by catalpol suppresses lipopolysaccharide-induced disruption of blood-brain barrier permeability. *Molecules*. 2018;23(9):2371. doi:10.3390/molecules23092371

29. Murakami M, Nakatani Y, Atsumi GI, et al. Regulatory functions of phospholipase A2. *Crit Rev Immunol*. 2017;37(2–6):127–195. doi:10.1615/CritRevImmunol.v37.i2-6.20

30. Cao D, Xu C, Xue Y, et al. The therapeutic effect of Ilex pubescens extract on blood stasis model rats according to serum metabolomics. *J Ethnopharmacol*. 2018;227:18–28. doi:10.1016/j.jep.2018.08.026

31. Yuan Z, Yang L, Zhang X, et al. Mechanism of Huang-lian-Jie-du decoction and its effective fraction in alleviating acute ulcerative colitis in mice: regulating arachidonic acid metabolism and glycerophospholipid metabolism. *J Ethnopharmacol*. 2020;259:112872. doi:10.1016/j.jep.2020.112872

32. Fijneman RJ, Cormier RT. The roles of sPLA2-IIA (Pla2g2a) in cancer of the small and large intestine. *Front Biosci*. 2008;13:4144–4174. doi:10.2741/2998

33. Boyanovsky BB, Webb NR. Biology of secretory phospholipase A2. *Cardiovasc Drugs Ther*. 2009;23(1):61–72. doi:10.1007/s10557-008-6134-7

34. Grönroos JO, Laine VJ, Nevalainen TJ. Bactericidal group IIA phospholipase A2 in serum of patients with bacterial infections. *J Infect Dis*. 2002;185(12):1767–1772. doi:10.1086/340821

35. Murakami M. Lipid mediators in life science. *Exp Anim*. 2011;60(1):7–20. doi:10.1538/expanim.60.7

36. Beck S, Lambeau G, Scholz-Pedretti K, et al. Potentiation of tumor necrosis factor alpha-induced secreted phospholipase A2 (sPLA2)-IIA expression in mesangial cells by an autocrine loop involving sPLA2 and peroxisome proliferator-activated receptor alpha activation. *J Biol Chem*. 2003;278(32):29799–29812. doi:10.1074/jbc.M211763200

37. Schrör K. Aspirin and platelets: the antiplatelet action of aspirin and its role in thrombosis treatment and prophylaxis. *Semin Thromb Hemost*. 1997;23(4):349–356. doi:10.1055/s-2007-996108

38. Jin Y, Xie Z, Li S, et al. Combined lipidomics and network pharmacology study of protective effects of Salvia miltiorrhiza against blood stasis syndrome. *Evid Based Complement Alternat Med*. 2021;2021:5526778. doi:10.1155/2021/5526778

39. Liu Y, Zhong H, Xu P, et al. Deciphering the combination mechanisms of Gualou-Xiebai herb pair against atherosclerosis by network pharmacology and HPLC-Q-TOF-MS technology. *Front Pharmacol*. 2022;13:941400. doi:10.3389/fphar.2022.941400

40. Ren P, Cao JL, Lin PL, et al. Molecular mechanism of luteolin regulating lipoxygenase pathway against oxygen-glucose deprivation/reperfusion injury in H9c2 cardiomyocytes based on molecular docking. *Zhongguo Zhong Yao Za Zhi*. 2021;46(21):5665–5673. doi:10.19540/j.cnki. cjcmm.20210805.701